atmosphere

MDPI

Article

Simulation of Northern Winter Stratospheric Polar Vortex Regimes in CESM2-WACCM

Dong Guo [1], Zhuoqi Liang [1,*], Qiang Gui [2], Qian Lu [1], Qiong Zheng [2] and Shuyang Yu [1]

[1] Collaborative Innovation Center on Forecast and Evaluation of Meteorological Disasters (CIC-FEMD), Key Laboratory of Meteorological Disaster, Ministry of Education (KLME), Joint International Research Laboratory of Climate and Environment Change (ILCEC), Nanjing University of Information Science and Technology, Nanjing 210044, China
[2] Meteorological Bureau of Baiyin, Baiyin 730900, China
* Correspondence: liangzhuoqi@nuist.edu.cn

Abstract: The possible impact of various Arctic polar vortex regimes for the stratosphere on the Northern Hemisphere extratropics has not been fully understood. Previous study has classified the stratospheric Arctic vortex to six regimes using the k-mean clustering algorithm based on the ERA5 reanalysis. The stability and robustness of the classification is further verified with a much longer model dataset and historical integrations from CESM2-WACCM. Consistent with the reanalysis, we clustered the Arctic stratospheric polar vortex forms into six patterns, named as homogeneously-intensified and -weakened regimes (HI, HW), North America-intensified and -weakened regimes (NAI, HAW), and Eurasia-intensified and -weakened regimes (EUI, EUW). A zonally uniform positive (negative) Northern Annular Mode (NAM) pattern develops during the HI (HW) regime from the stratosphere to troposphere. The NAM-like pattern shifts toward the western hemisphere with the largest negative (positive) anomalous height center shifting to North America during the NAI (NAW) regime. In contrast, the maximum polar anomaly center moves towards polar Eurasia during the EUI (EUW) regime. The HI, NAI, and EUW regimes are accompanied with weakened wave activities, while the HW, NAW, and EUI regimes are preceded by enhanced planetary waves. Accordingly, persistent anomalies of warmth (coldness) exist over midlatitude Eurasia and North America during the HI (HW). Anomalous warmth (coldness) centers exist in northern Eurasia, while anomalous coldness (warmth) centers exist around the Mediterranean Sea during the NAI (NAW) regime. Anomalous warmth (coldness) centers develop in East Asia in the EUI (EUW) periods. The rainfall anomaly distributions also vary with the stratospheric polar vortex regime. The frequency for stratospheric regimes during SSWs and strong vortex events is also assessed and consistent with previous findings.

Keywords: stratospheric polar vortex; regimes; CESM2-WACCM; eddy heat flux

check for updates

Citation: Guo, D.; Liang, Z.; Gui, Q.; Lu, Q.; Zheng, Q.; Yu, S. Simulation of Northern Winter Stratospheric Polar Vortex Regimes in CESM2-WACCM. *Atmosphere* **2023**, *14*, 243. https://doi.org/10.3390/atmos14020243

Academic Editor: Yoshihiro Tomikawa

Received: 2 December 2022
Accepted: 24 January 2023
Published: 26 January 2023

Copyright: © 2023 by the authors. Licensee MDPI, Basel, Switzerland. This article is an open access article distributed under the terms and conditions of the Creative Commons Attribution (CC BY) license (https://creativecommons.org/licenses/by/4.0/).

1. Introduction

The northern winter polar vortex at the Arctic stratosphere is disturbed by augmented waves for upward propagation from the upper troposphere and exhibits different shapes [1–3]. The importance of the polar vortex on the stratosphere-troposphere coupling has been widely noticed, and changes in the geographic location and intensity of the polar vortex at Arctic stratospheric are related to various tropospheric circulation anomaly states [4–6]. Recently, some studies have established the possible linkage between the stratospheric polar vortex state and local atmospheric environment [3,7–9]. For example, Lu et al. [9] found that the subseasonal variability in the atmospheric particulate during the sudden stratospheric warming events (e.g., extreme weak stratospheric polar vortex events) is usually enhanced as compared with the stratospheric dormant periods. In contrast, the strengthened polar vortex at the stratosphere is associated with anomalous warming signals in the North Pacific and northern Eurasia [10–13].

The SSW event, as a typical representative for the weakened stratospheric polar vortex, results from sharply strengthened wave activities from troposphere to stratosphere [14–16]. The negative Northern Annular Mode (NAM) phase projects from the weakened Arctic polar vortex at the stratosphere, which can sustain to influence the near surface climate in a pressure pattern resembling the negative Arctic Oscillation phase [17,18]. In contrast, the strengthened Arctic polar vortex at the stratosphere shows a positive NAM response [10,11,13]. The NAM signal can propagate downward from the stratosphere to troposphere and increase the probability to better predict the near surface weather on an amplified time scale [12,19–23]. Therefore, the different stratospheric polar vortex states might exert various influence on the tropospheric weather condition and provide a predictive causation of the near surface weather on a longer time scale [18,23–25].

Extreme weather events that affect human production and survival often occur in those specific circulation patterns, which are the so-called weather regimes [6,26,27]. The concept of weather regimes has been documented for long time [28,29]. Therefore, understanding the relationship between extreme conditions at extratropic regions and stratospheric weather regimes might be conducive to legitimately predict weather in a longer period of lead time [27,30–32]. To better group the stratospheric weather patterns and to facilitate a deeper investigation for the effects of inequable stratospheric Arctic vortex shapes on the troposphere or the near surface, the k-means method can be utilized to classify the northern winter circulation in the stratosphere [25]. Kretschmer et al. [33] established the possible relation between different polar vortex regimes at the stratosphere and the extreme coldness in the Northern Hemisphere continents. Lee et al. [27] clustered the tropospheric weather circulation states over the Pacific-North America region and tried to establish a possible linkage between tropospheric weather regimes and stratospheric Arctic vortex patterns. Various Arctic stratospheric polar vortex regimes connected to sea ice variability over Arctic, and changes of the regime frequencies probably arisen from the secular deficit tendency of the sea ice over the Arctic are reported [34].

Most recently, Liang et al. [6] divided the stratospheric Arctic vortex into several patterns, but they used the limited reanalysis to establish the linkage between the Arctic vortex appearances and the tropospheric circulation changes. The robustness and stability of the stratospheric regimes is still required to further verify using a large sample. The reproducibility of SSWs was widely assessed for some individual models or multiple models, which participated in the Coupled Model Intercomparison Project Phases 5 and 6 (CMIP5/6) [35–38]. Liang et al. [39] identified that some facets of the SSWs are reasonably reproduced by CESM2-WACCM, and the stratospheric variability is also more realistically reproduced by this model than most CMIP5/6 models [1,37,38,40]. Yu et al. [13] evaluated the Arctic ozone loss events in CESM2-WACCM and found that the ozone loss is always accompanied by a strong polar vortex event in both observations and models [11]. However, we still do not know clearly if the polar vortex regimes extracted from the reanalysis can be simulated by the state-of-the-art model. As CESM2-WACCM can well simulate the stratospheric variability similarly to SSWs [39], simulation of stratospheric polar vortex regimes by CESM2-WACCM is assessed in this study.

In this study, the Arctic vortex regimes in the stratosphere from CESM2-WACCM will be clustered, although difference might exist between the reanalysis and the model. Using a longer dataset, the relationship between the extratropical temperature and precipitation and the Arctic vortex regimes in the stratosphere can be better established. The remaining of the paper is organized as follows. The data and methods utilized in this study are described in Section 2. The simulation of extratropical circulation pattern relating to different northern winter polar vortex regimes at the stratosphere is described in Section 3. The relationship between stratospheric regimes and changes in wave activities is shown in Section 4. The probable effect of the stratospheric Arctic vortex regimes on lower levels and near the surface is examined in Section 5. At last, in Section 6, conclusions are discussed.

2. Datasets and Methodology

2.1. Model and Simulations

Three historical simulations during 1850–2014 from CESM2-WACCM were employed. CESM2-WACCM participated in phase 6 of the Coupled Model Intercomparison Project (CMIP6). CESM2-WACCM is a fully coupled earth system model, which integrates land, atmosphere, river, ocean, land-ice, sea-ice, and ocean-wave trough the coupler [38,41–43]. In CESM2-WACCM, the horizontal resolution is 1.25° (longitude) × 0.9° (latitude), and the vertical layer extend from the near surface to ~4.5×10^{-6} hPa at 70 sigma/pressure levels.

2.2. Methodology

2.2.1. Clustering

For extracting the daily states of polar vortex at the stratosphere, daily geopotential height anomalies at 50 hPa from 60° N poleward in the extended winter season (November-March) for all days are clustered using the Python package scikit-learn with k = 6. We then assigned all days to a regime according to their minimum Euclidean distance to the cluster centroids. The number of the clustering k is confirmed by the total square error (SSE). The estimated squared error is expressed as $\mathrm{SSE} = \sum_{i=1}^{k} \sum_{p_{i,j} \in c_i} \left| p_{i,j} - m_i \right|^2$, in which C_i is the cluster ranked i, m_i denotes the average of all samples in C_i termed the centroid of C_i, $P_{i,j}$ is a sample in the C_i group, ranked j. The clustering errors in all samples are represented by SSE, which indicates the quality of clustering result. As the cluster number k increases, the division of sample will be more refined, and the degree of aggregation for each cluster will progressively rise, so the sum of error squares SSE will be smaller as expected. Furthermore, if k is less than the real clusters number, the increasing of k enlarges the degree of aggregation for the clusters to a large extent, and the attenuation of SSE will be extremely huge. The degree of aggregation for clustering received by increasing k will decline swiftly, while k attains the ideal cluster number. Meanwhile, with the constant increasing of k, the decay of SSE will slow down rapidly. After that, the attenuation of SSE tends to level off. At this time, k is the real number of clusters for the data. To keep consistent with the previous study [6], k is set to 6. After k is determined, all the instantaneous structures are grouped into the six clusters, and an instantaneous structure only corresponds to one of the six clusters, which is very different from the empirical orthogonal function analysis (EOF). In an EOF study, an instantaneous structure can be composed of different EOF modes with varying contributions.

2.2.2. Strong Polar Vortex Events

Once the zonally averaged westerlies in the 55–75° N latitude band exceed 40 m/s and afterward sustain for >20 days, an extremely strong Arctic vortex event is identified for CESM2-WACCM. The first day exceeding this value is considered as the central day (day 0) for strong Arctic vortex events. Eventually, 391 strong polar vortex events in total are picked from a 495-year dataset (165 years for a historical run, three runs available).

2.2.3. Extreme Weak Polar Vortex Events

The extreme weak polar vortex event (or SSW) is determined by the date when the zonal average zonal wind on the 10 hPa isobaric surface at 60° N changes from west to east wind [14]. The first day is defined as day 0 of the SSW date. Once the SSW is determined, due to the huge perturbation of the circumpolar wind after the SSW starts, no SSW is selected in the following 20 days. Using the 495-year data, a total of 228 major SSWs are searched.

2.2.4. Eliassen Palm Flux

To well diagnose the vertical transmission of planetary waves between the stratosphere and troposphere, the Eliassen Palm (EP) flux is used in this study [44,45]. The vertical component of the EP flux,

$$F_z = \rho_0 a\, cos\varnothing \{ \frac{\overline{v'\theta'}}{\partial\overline{\theta}/\partial z} [f - \frac{1}{a\, cos\varnothing} \frac{\partial}{\partial\varnothing} (\overline{u}\, cos\varnothing)] - \overline{u'w'} \},$$

where a is the radius of the Earth, θ is potential temperature, $\rho_0 = \rho_s exp(-z/H)$ is the standard density in log-pressure coordinates, ρ_s is the sea-level reference density, $\varnothing$ is latitude, f is the Coriolis parameter, H is the scale height, the overbar denotes zonal average, prime denotes the departure from zonal mean. F_z can be calculated to represent the upward propagation of planetary waves.

3. Stratospheric Weather Regimes in the Northern Winter

3.1. Simulation of the Six Regimes at the Stratosphere by CESM2-WACCM

The k-means clustering algorithm is used to identify stratospheric polar vortex regimes for three historical simulations during 1850–2014 from CESM2-WACCM. Consistent with previous study [6], the 50 hPa geopotential height anomalies on 60–90° N latitude bands are divided into six clusters, which are shown in Figure 1. The proportion of the six clusters are 0.19, 0.08, 0.17, 0.19, 0.19, and 0.18, respectively. The first cluster is a homogeneously intensified (HI) stratospheric polar vortex regime covered over the Arctic (Figure 1a). Compared with the ERA5 reanalysis, the positive annular height anomalies at the midlatitudes are weaker in the model than in the reanalysis [6]. Conversely, the second regime corresponds to a homogeneously weakened (HW) polar vortex at the stratosphere covered over the Arctic (Figure 1d). The polar vortex intensifies and displaces to the North American continent (NAI) for the third cluster, while the vortex in the fourth cluster is weakened with the largest positive anomalies centered over the Arctic Ocean in the western hemisphere (NAW) (Figure 1b,e). In the fifth grouping, the Arctic vortex intensifies and displaces toward to the eastern hemisphere (EUI) (Figure 1c), while in the sixth cluster, the vortex displaces toward North Atlantic, with the geopotential height in northern Eurasia increasing (Figure 1f). Compared with the ERA5 reanalysis, the simulated polar vortex for the sixth cluster is biased further eastward [6]. The weakened polar vortex observed in northern Eurasia (EUW) shifts farther eastward to the Russia-Bering Strait (Figure 1f). Therefore, the model simulates a HI and a NAW regime internally different from the reanalysis. Most models tend to simulate an over-strong and over-large stratospheric polar vortex, and this bias has been shown to lead to less SSWs [46]. The bias in the simulated HI and EUW regimes are likely associated with the over-strong polar vortex and underestimated planetary waves in models, left for a future study. The sensitivity of the clustering to the timespan is also tested, and the clustering during the full timespan and the subsampling (e.g., 1950–2014) are nearly identical.

3.2. Wave Forcing during Six Polar Vortex Regimes at the Stratosphere

Previous studies indicated that planetary waves explain the variability of the Arctic vortex at the stratosphere [2,14,47–50]. To exam the wave forcing during those regimes, the vertical cross-section of composited F_z anomalies is shown in Figure 2. For HI, NAI and EUW pattern, the negative F_z anomalies dominate at higher latitudes extending throughout the troposphere and the stratosphere (Figure 2a,b,f). This implies that weakening of the upward propagations of waves are a necessary condition for the homogeneously-intensified, North America-intensified, and Eurasia-weakened polar vortex events. The wave forcing anomaly is smaller for EUW than HI and NAI regimes.

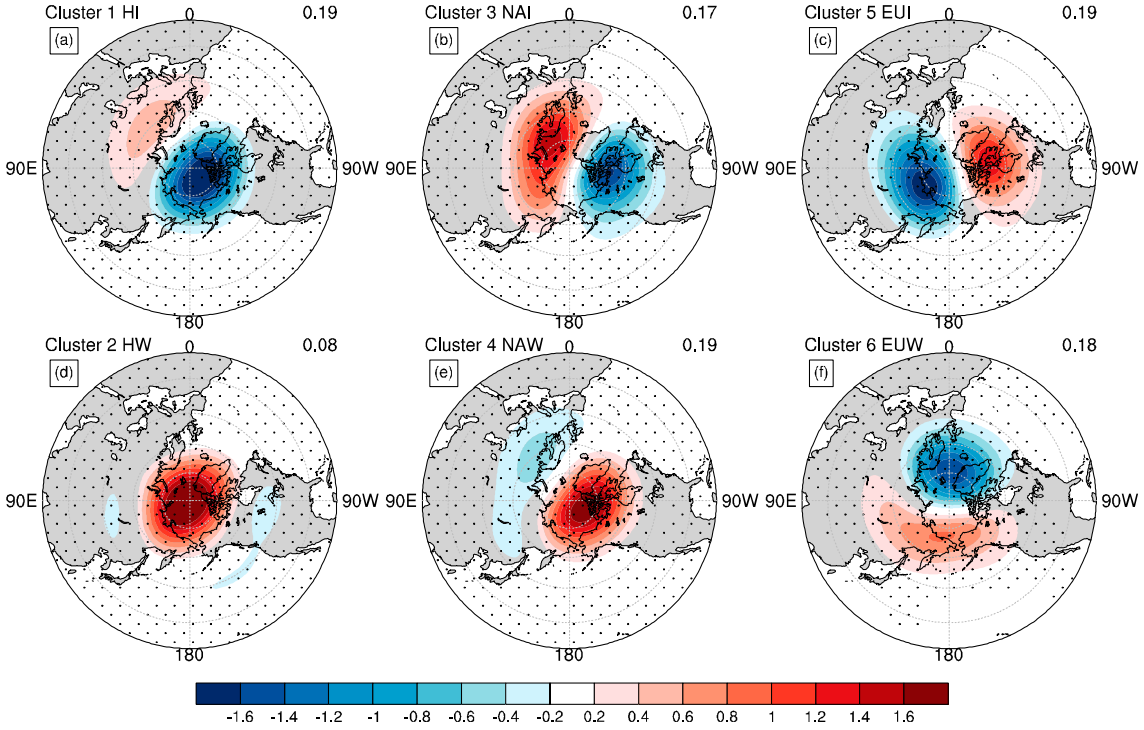


Figure 1. (**a**–**f**) Composited 50 hPa standardized geopotential height anomalies for the six stratospheric Arctic vortex weather regimes (shading) over 20–90° N based on the historical run. The dotted area marks the composite anomalies significant at the 99% confidence level based on a two-sided Student's *t*-test. The top right of each plot also shows the frequency proportion for each regime.

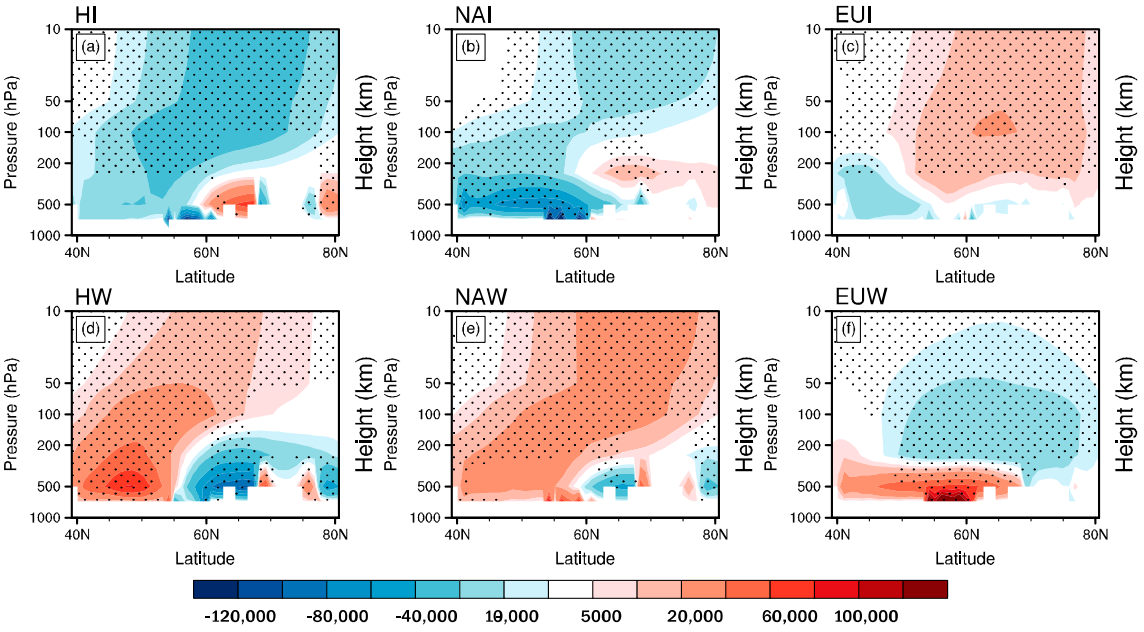


Figure 2. (**a**–**f**) Composited F_z anomalies by total waves (units: Pa m^2/s^2) for the six stratospheric Arctic vortex regimes from the historical runs. The dotted area manifests the composited eddy heat flux anomalies at the 99% confidence level based on a two-sided Student's *t*-test.

The other three regimes, EUI, HW, and NAW are preceded by anomalously stronger waves throughout the troposphere and the stratosphere (Figure 2c–e). Further, the EUI regime showed a narrower region with anomalously upward propagation of waves than HW and NAW regions (50–90° N vs. 40–90° N). The enhanced eddy heat flux for HW

shows a stronger maximum center than the EUI and NAW regimes, which appears in the middle troposphere in the latitude band over 40–55° N.

3.3. Simulation of Tropospheric Circulation Patterns for the Six Regimes at the Stratosphere

The composite 500 hPa standardized geopotential height anomalies during six Arctic stratospheric regimes are shown in Figure 3 for CESM2-WACCM. The potential impact of the stratospheric regimes on tropospheric circulation in CESM2-WACCM is basically consistent with the ERA5 reanalysis. Specifically, the tropospheric geopotential height anomalies display three pairs of opposite patterns. As to the HI (HW) weather regime, a positive (negative) NAM-like pattern develops at northern mid-to-high latitudes. The geopotential heights anomalously decrease (increase) over the North Pole, whereas a long and narrow patch of positive (negative) height anomalies appear in midlatitudes, with three significant anomaly centers over Lake Baikal, North Atlantic-western Europe, and Great Lakes (Figure 3a,d). As to the NAI (NAW) at the stratosphere, the tropospheric positive (negative) NAM-like circulation pattern shifts towards North America; meanwhile, the positive (negative) height anomaly band over northern Eurasia is biased farther poleward (Figure 3b,e). For EUI, the polar vortex shifts toward northern Eurasia, contrasted with a positive height anomaly center over Arctic Canada (Figure 3c). The last clustering is a dipole pattern between Arctic Russia and Alaska (Figure 3f), and this extracted pattern is inconsistent with the result from the reanalysis, which exhibits an opposite pattern to the EUI. Compared with the ERA5, this pattern is farther westward shifted, and for easy description it is still termed EUW. In short, the tropospheric geopotential height anomalies during the six regimes are generally consistent with the result from ERA5 reanalysis [6].

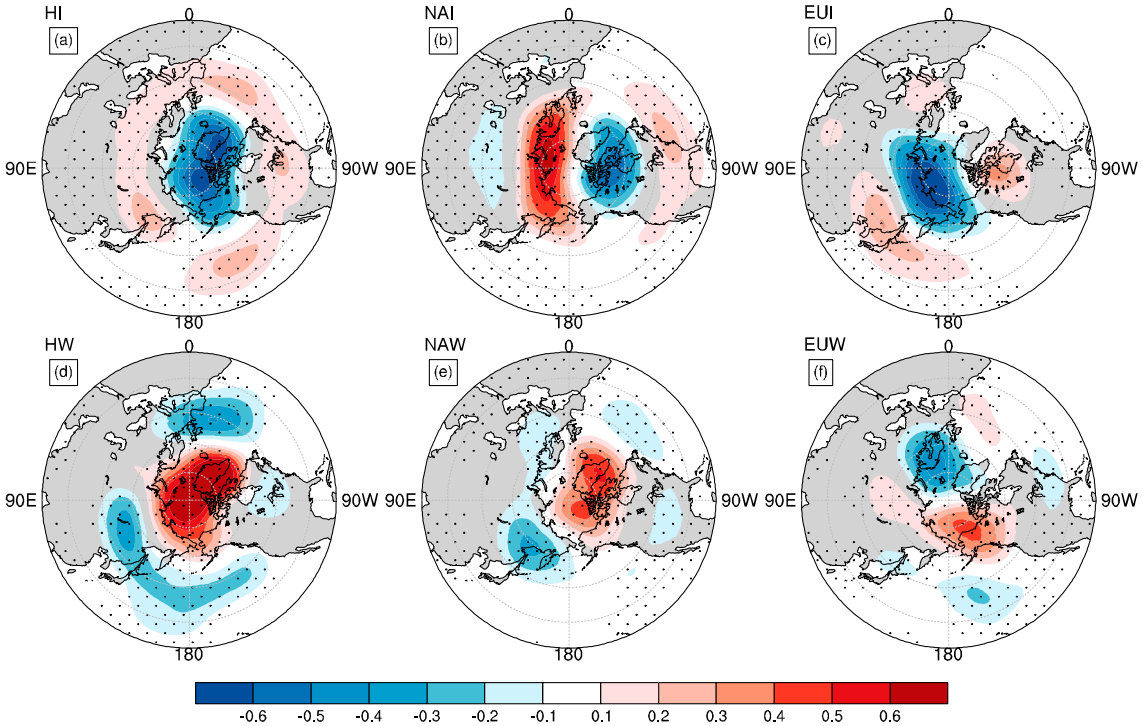


Figure 3. (**a**–**f**) Composited standardized 500 hPa height anomalies for the six stratospheric Arctic vortex weather regimes (shading) over 20–90° N based on the historical run. The dotted area marks the composited anomalies at the 99% confidence level based on a two-sided Student's *t*-test.

4. Evolution of the Tropospheric Circulation Related to the Regimes in the Stratosphere

4.1. Change in the Circulation at the Stratosphere

The composited evolution of the 50 hPa standardized height anomalies for the six Arctic regimes at the stratosphere from CESM2-WACCM simulations is shown in Figure 4. Three periods are focused for each stratospheric regime, namely the initial stage (from −30 to −10 days), the mature stage (from −10 to 10 days), and the decay stage (from 10 to 30 days). In comparison with the ERA5 reanalysis, negative (positive) weak height anomalies at the North Pole coexist with positive (negative) anomalies over the Asia-Pacific sector during the HI (HW) initial stage, corresponding to the typical positive (negative) NAM pattern (Figure 4(a1–a3,b1–b3)). During the mature phase of HI (HW), negative (positive) geopotential height anomalies exist over the Arctic Ocean, whereas positive (negative) height anomalies in midlatitudes develop to its peak. The HI (HW) pattern is nearly unchanged although the intensity gradually weakens. The timescale for HI (HW) regime is rather persistent and lasts for nearly two months.

In contrast, the evolution of the NAI (NAW) is fast, and the height anomaly patterns during the three periods are different (Figure 4(c1–c3,d1–d3)). The negative (positive) height anomalies develop over the northern Eurasia in the initial stage, and move towards North America in the mature phase, contrasted with positive (negative) height anomalies in the northern part of Eurasia. During the decaying period, the NAI (NAW) pattern weakens quickly, and the maximum anomaly center move out of North America.

In the EUI (EUW) initial period, the negative anomalies are simulated over parts of North Pole, and the EUI (EUW) pattern is still not clearly present (Figure 4(e1–e3,f1–f3)). In the mature stage, geopotential heights decrease (increase) over part of Arctic Eurasia, which are contrasted with positive (negative) anomalies over parts of Arctic Canada and Greenland. This pattern shifts eastward and gradually diminishes in the decaying period, with positive (negative) height anomalies shifting to North Atlantic-Europe and negative (unclear) height anomalies over North America.

4.2. Change in the Tropospheric Circulation

To test the evolution of the tropospheric height anomalies corresponding to various regimes at the stratosphere, the composited 500 hPa standardized height anomalies for stratospheric Arctic vortex weather regimes from CESM2-WACCM for three periods are displayed in Figure 5. In the HI (HW) weather regime, the stratospheric positive (negative) NAM like response develops deep downward to the troposphere (Figure 5(a1–a3,b1–b3)). Specifically, negative (positive) geopotential height anomalies form over the North Pole, which are contrasted with a long band of positive (negative) midlatitude height anomalies. This midlatitude anomaly band is divided into two centers, one over North Pacific, and the other over North Atlantic. The positive (negative) NAM pattern has a longer timescale and show very similar height anomaly distribution from the early stage to the recession stage.

In the NAI (NAW) weather regime, negative (positive) geopotential anomalies form in the western hemisphere, while positive (negative) anomalies appear in some part of the eastern hemisphere (Figure 5(c1–c3,d1–d3)). The negative (positive) height anomalies move eastward to Arctic Canada-Greenland, while a long band of positive (negative) anomalies form in midlatitudes. This pattern resembles the NAM but with the lobes in the eastern hemisphere situated further north. In the decaying stage, the largest anomalies move out of North America, and the general pattern also largely weakens.

For the EUI (EUW) regime, positive (negative) anomalies initially appear over North Pacific, and continental anomalies are fairly weak (Figure 5(e1–e3,f1–f3)). The largest negative (positive) anomalies cover the northern part of Eurasia (Bering Strait), and the dipole pattern over Asia-Pacific is more evident than that over North America-the Atlantic Ocean in the mature stage. The largest height anomaly centers move to oceans and largely weaken.

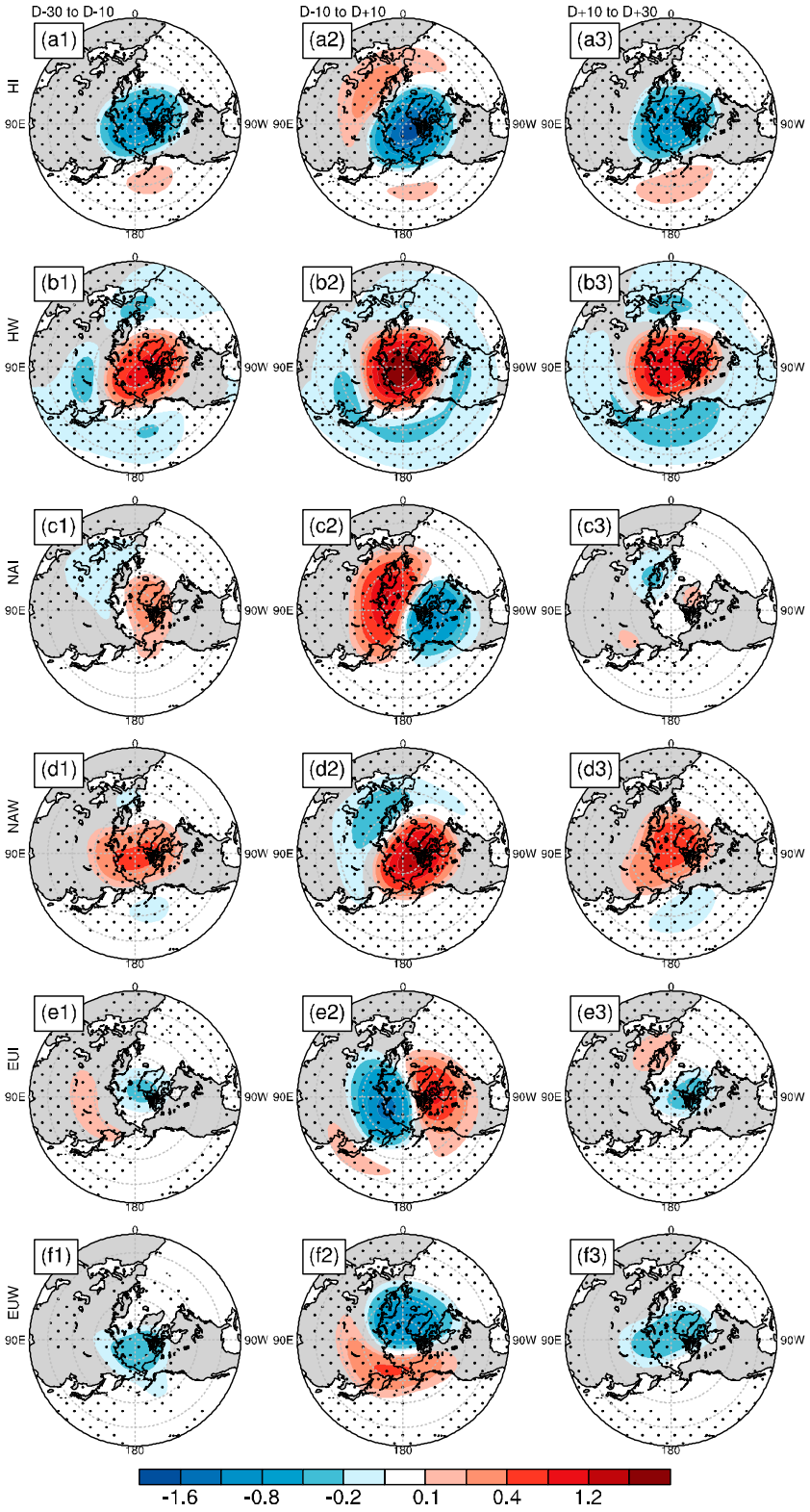


Figure 4. Composited leading/lagging evolutions of the standardized 50 hPa geopotential height anomalies (shading) during three stages from 20 to 90° N for six stratospheric Arctic vortex weather regimes based on three historical runs. (**a1**–**f3**) The clusters 1–6 are printed as HI, HW, NAI, NAW, EUI, and EUW regimes, respectively. The first column displays the average for days −30 to −10, the second column displays the average for days −10 to 10, and the third column displays the average for days 10 to 30. The dotted area indicates the composited anomalies significant at the 99% confidence level based on a two-sided Student's *t*-test.

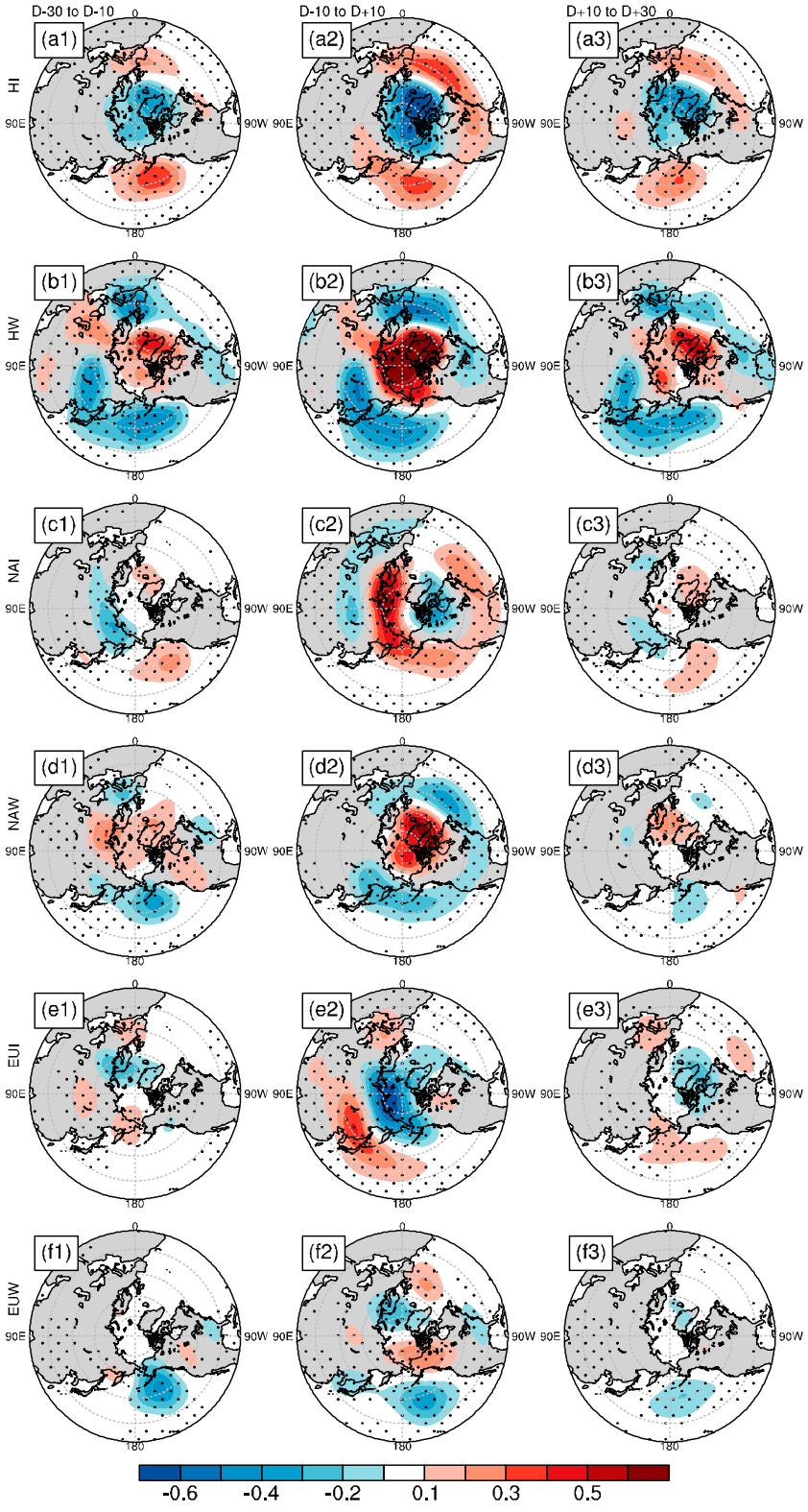


Figure 5. Composited leading/lagging evolutions of standardized 500 hPa geopotential height anomalies (shading) during three stages from 20 to 90° N for six stratospheric Arctic vortex weather regimes. (**a1**–**f3**) The clusters 1–6 are printed as HI, HW, NAI, NAW, EUI, and EUW regimes, respectively. The first column displays the average for days −30 to −10, the second column displays the average for days −10 to 10, and the third column displays the average for days 10 to 30. The dotted area indicates the composited anomalies significant at the 99% confidence level.

4.3. Change in the Weather Anomalies at Near Surface

The composite 850 hPa standardized temperature anomalies are shown in Figure 6 in the three periods for each stratospheric regime. In the HI (HW) weather regime, the cold (warm) Arctic-warm (cold) continent pattern is evidently present from the initial to decaying period, implying a positive long-lasting downward impact of the HI (HW) regime. Warm (cold) temperature anomalies exit in most parts of the land in the eastern hemisphere, and the Arctic Ocean is dominated by cold (warm) temperature anomalies (Figure 6(a1–a3,b1–b3)). Warm (cold) temperature anomalies are not clear in the initial stage but appear in the mature stage with maximum center bias to Great Lakes. In contrast, positive (negative) temperature anomalies in East Asia are stronger and more long-lasting.

For the NAI (NAW) regime, warm (cold) temperature anomalies over East Asia and cold (warm) temperature anomalies over Arctic begin to develop in the initial stage (Figure 6(c1–c3,d1–d3)). As the polar vortex is biased to North America in the mature stage, cold (warm) temperature anomalies appear over North Canada, while the eastern hemisphere land is covered with a dipole pattern with warm (cold) temperature anomalies in Arctic Russia and cold (warm) anomalies around midlatitude Eurasia. During the decaying period, the anomaly pattern largely shrinks and diminishes.

In the EUI (EUW) regime, warm temperature anomalies are preceded over north Asia (Canada) (Figure 6(e1–e3,f1–f3)). As the polar vortex strengthens (weakens) over Eurasia, negative (positive) temperature anomalies appear over Arctic Russia, while positive (negative) temperature anomalies exist over East Asia. The EUI (EUW) evolves quickly and nearly disappear in the decaying period.

Similarly, the composited precipitation anomalies for each stratospheric Arctic vortex regime are shown in Figure 7. In the HI (HW) weather regime, from the initial to the mature period, organized and remarkable precipitation anomalies principally appear in the Europe and North Atlantic. Less (more) rainfall occurs in North Atlantic-southern Europe and northeast Pacific, whereas positive (negative) precipitation anomalies cover northern Europe and East Asia (Figure 7(a1–a3,b1–b3)). In the NAI (NAW) weather regime, less (more) precipitation anomalies form over northeast Pacific, North Atlantic and northern Europe during the mature stage, and rainfall anomalies in the other two periods are less organized (Figure 7(c1–c3,d1–d3)). In the EUI (EUW) weather regime, less (more) precipitation covers North Pacific, and the composite rainfall signals are fairly weak across the globe (Figure 7(e1–e3,f1–f3)).

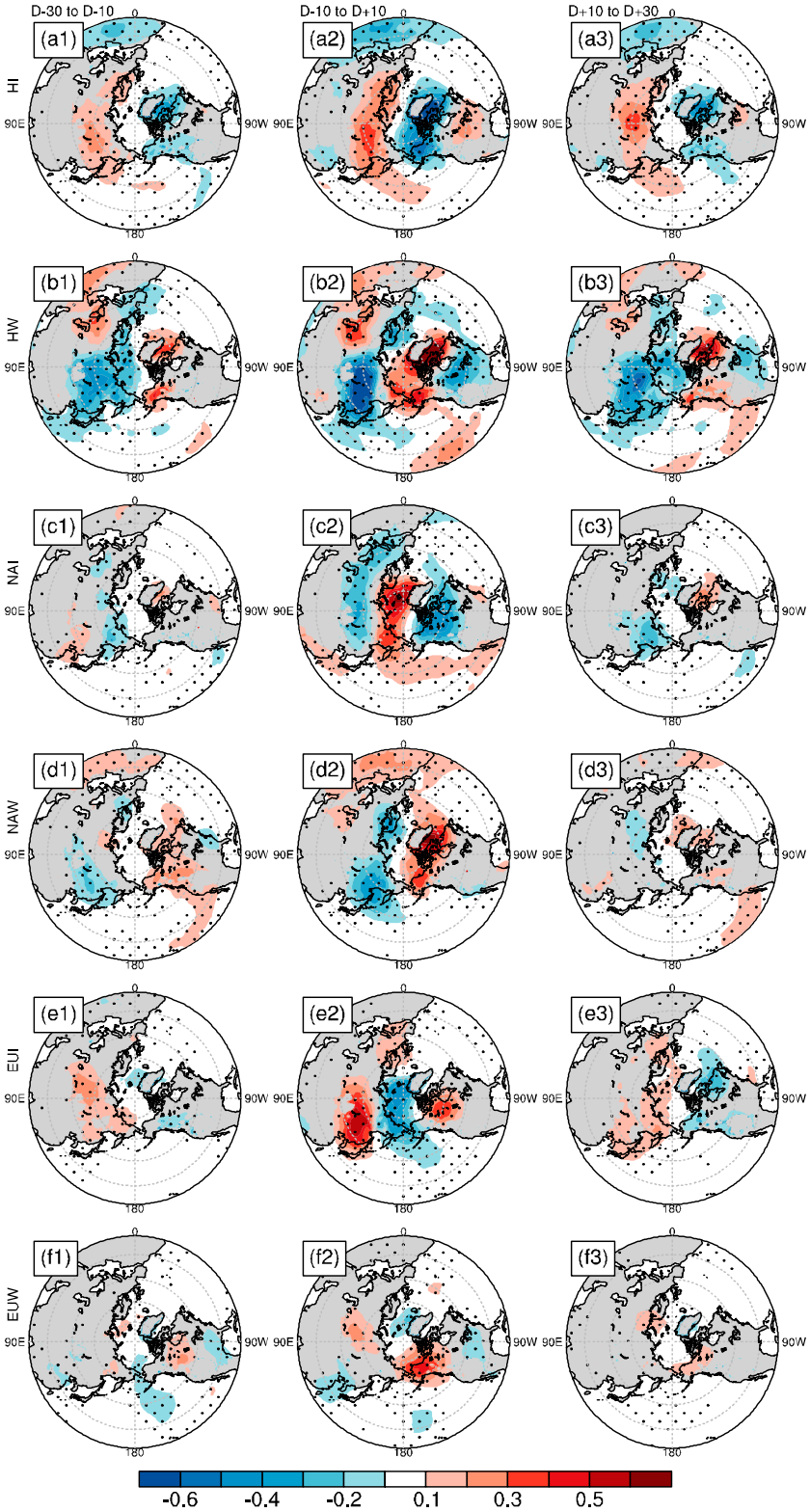


Figure 6. Composited leading/lagging evolutions of the standardized 850 hPa temperature anomalies (shading) from 20 to 90° N during three stages of the six stratospheric Arctic vortex weather regimes. (**a1**–**f3**) The clusters 1–6 are printed as HI, HW, NAI, NAW, EUI, and EUW regimes, respectively. The first column displays the average for days −30 to −10, the second column displays the average for days −10 to 10, and the third column displays the average for days 10 to 30. The dotted area indicates the composited anomalies significant at the 99% confidence level.

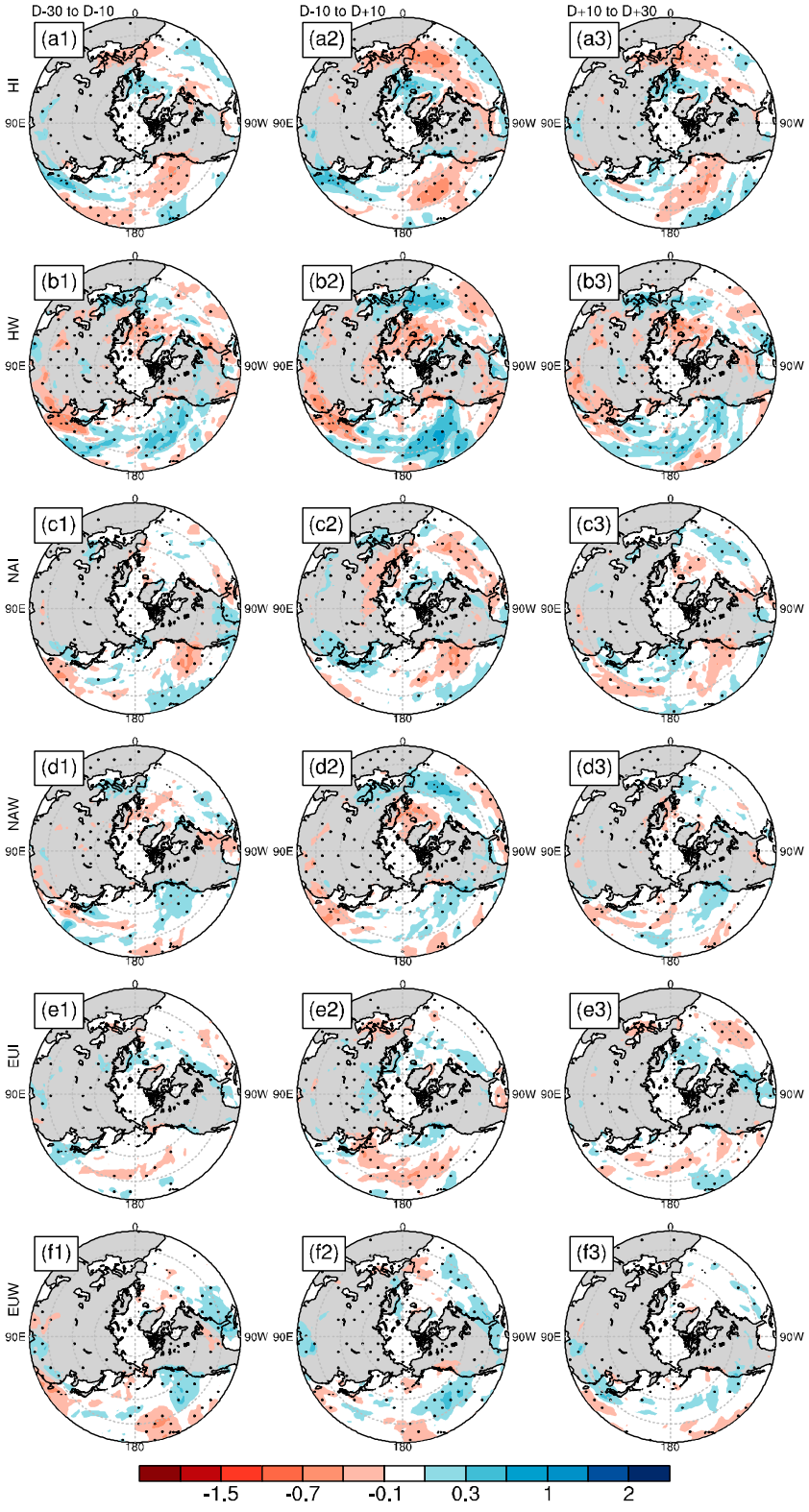


Figure 7. Composited leading/lagging evolutions of precipitation anomalies (shadings; units: mm/d) from 20 to 90° N during three stages of the six stratospheric Arctic vortex weather regimes. (**a1**–**f3**) The clusters 1–6 are printed as HI, HW, NAI, NAW, EUI, and EUW regimes, respectively. The first column displays the average for days −30 to −10, the second column displays the average for days −10 to 10, and the third column displays the average for days 10 to 30. The dotted area indicates the composited anomalies significant at the 99% confidence level.

5. Stratospheric Weather Regime Conversions during Vortex Extremes

5.1. Stratospheric Weather Regime Conversion during SSWs

Liang et al. [6] revealed that the stratospheric regimes converse during stratospheric vortex extremes using the reanalysis. Further, the evolution of the composite regime frequency for SSW is shown in Figure 8. Four periods for SSWs are considered, including −20~−1 days (P1), 0~20 days (P2), 21~40 days (P3), and 41~60 days (P4). The date of SSW start is considered as day 0, and the period during −20~60 days are concerned. The statistics are based on 228 total SSWs and 729 total SPVs from three historical experiments during 1850–2014.

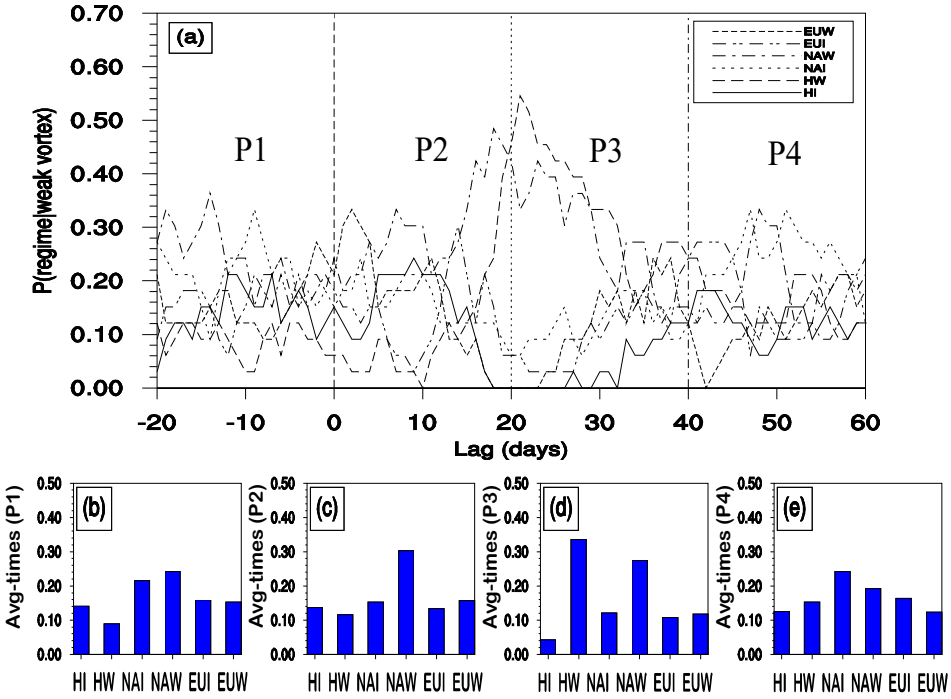


Figure 8. (**a**) The occurrence frequency statistics for the six stratospheric Arctic vortex weather regimes within days −20 to 60 with respect to the SSW occurrence date based on three historical runs. (**b**–**e**) The mean proportion of each polar vortex regimes at the stratosphere for four sub-stages: days −20 to −1 (P1), days 0 to 20 (P2), days 20 to 40 (P3), and days 41 to 60 (P4).

During the early stage for SSWs (P1), the NAW regime dominates, and the frequencies of the remaining five stratospheric regimes are comparable (Figure 8a,b). Further, the total frequency of the weak Arctic vortex regimes (HW, NAW, and EUW) is larger than that of the strong Arctic vortex regimes (HI, NAI, and EUI). This might imply that the polar vortices show a detectable dependence on the regime in the initial stage of SSWs. The NAW regime increases rapidly in the P2 period, account for ~30% of the total days within 30 days following SSW onsets (Figure 8a,c). Namely, the stratospheric Arctic vortex moves out of the North Pole and days with the vortex intensity decrease over North America ranks the first out of all regimes. The stratospheric polar vortex weakens rapidly with the proportion of the HW regime maximized (>0.3) during P3 period (days after SSW onset) (Figure 8a,d), which together with NAW and EUW, the weak polar vortex regimes appear most of days during this period. In the decaying stage of SSWs, frequencies of strong Arctic vortex regimes slowly recover with the NAI frequency higher than HI and EUI (Figure 8a,e). In general, the simulated evolution of the regime frequencies is consistent with the reanalysis.

5.2. Stratospheric Weather Regime Conversion during Strong Polar Vortex

The evolution of the composite stratospheric regime frequencies in the period of strong polar vortex events is shown in Figure 9. Similar to SSWs, four periods are focused for SPVs.

During the early stage and the fast grown period (P1 and P2), the HW regime accounts for a very small proportion and the proportion of HI increases rapidly. (Figure 9a-c). The HW, NAW and EUW regimes increase while the HI, NAI and EUI decrease at the mature stage (P3), implying that the stratospheric polar vortex may begin to weaken (Figure 9a,d). In the decaying period of SPVs, the stratospheric regimes frequencies are more uniformly distributed except the HI regime. The increasing of the frequency proportion for NAI and EUI and the decreasing for HI indicate that stratospheric polar vortex might shift to continent (Eurasia/North America) (Figure 9a,e). Compared with the ERA5 reanalysis data, it is found that the occurrence frequency of the six polar vortex regimes at the stratosphere during the SPVs are more stable during the four periods.

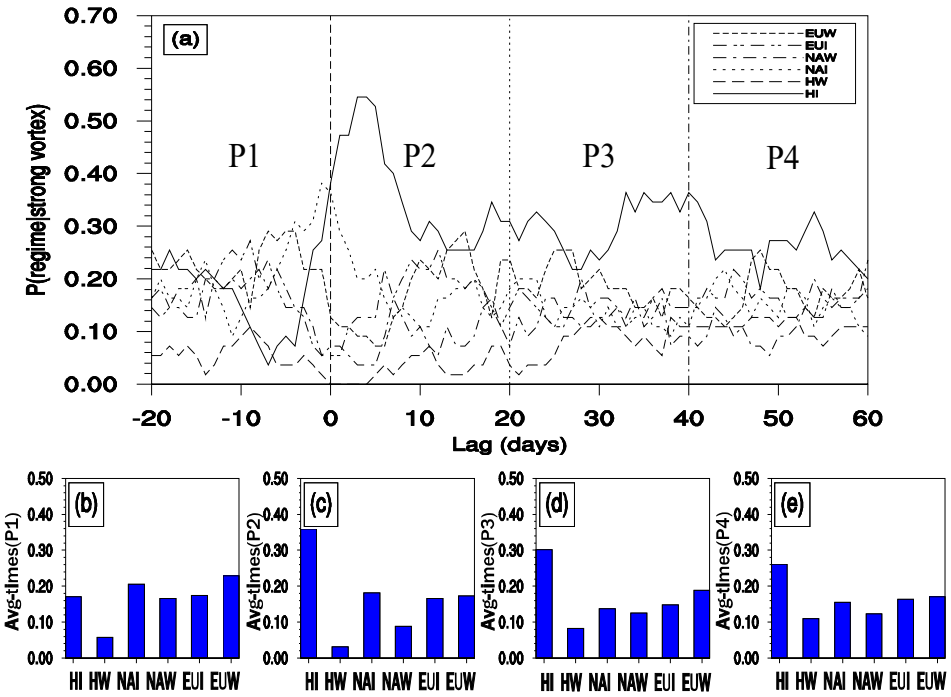


Figure 9. (**a**) The occurrence frequency statistics for the six stratospheric Arctic vortex regimes within days −20 to 60 with respect to the central date of strong stratospheric Arctic vortex events based on three historical runs. (**b**–**e**) The mean proportion of each polar vortex regimes at the stratosphere for four sub-stages: days −20 to −1 (P1), days 0 to 20 (P2), days 21 to 40 (P3), and days 41 to 60 (P4).

6. Conclusions

Following a previous study that classifies the stratospheric Arctic vortex into different regimes based on the reanalysis, this study continues to confirm the robustness of the six stratospheric Arctic vortex regimes using longer model data. Using the k-means method, the six regimes are also assessed for historical simulations. The frequencies of six stratospheric Arctic vortex regimes in historical simulations from CESM2-WACCM are similar to the reanalysis reported in a previous study [6]. The central positions and intensities of the six stratospheric circulation patterns are also basically consistent with the reanalysis, although centers of the EUW shifts farther eastward in historical simulations. The results from this study are as follows.

A zonally uniform positive (negative) NAM pattern develops for the stratospheric HI (HW) weather regime, which extend downward to the troposphere. Namely, the Arctic Ocean is dominated by a large patch of negative (positive) geopotential anomalies, while a long zonal band of positive (negative) geopotential anomalies exist in midlatitudes. The midlatitude band has two noticeable lobe centers, one over North Atlantic and one over East Asia. As to the NAI (NAW) regime, the general NAM pattern shifts toward the western hemisphere, and the maximum low (high) center is situated over North America, with the

positive height anomaly band in the eastern hemisphere biased to northern Eurasia. In contrast, for the EUI (EUW) regime, the NAM pattern shifts toward the eastern hemisphere, and the maximum Arctic center moves toward northern Eurasia, contrasted with positive (negative) geopotential anomalies over parts of North America. On average, the timescale of the HI (HW) regime is longer than that of the NAI (NAW) or EUI (EUW) regimes. The HI, NAI, and EUW regimes are forced by weakened wave activities, while the HW, NAW, and EUI regimes are driven by strengthened upward propagation of planetary waves.

In agreement with the circulation patterns, persistent warm (cold) temperature anomalies exist in midlatitude Eurasia and North America, and cold (warm) temperature anomalies develop over the Arctic Ocean during the HI (HW). The largest negative (positive) temperature anomaly center is biased farther northward in the western hemisphere to cover most of Canada during the NAI (NAW) weather regime, while warm (cold) temperature anomalies appear in northern Eurasia, contrasted with negative (positive) temperature around the Mediterranean Sea. The largest cold (warm) temperature anomaly center shifts to Arctic Russia, contrasted with warm (cold) anomalies in East Asia in the EUI (EUW) regimes.

The rainfall anomaly patterns also vary with the stratospheric Arctic vortex weather regimes. In the HI (HW) regime, organized dry (wet) anomalies form over Europe-North Atlantic and northeast Pacific, while wet (dry) anomalies form over parts of the Arctic Ocean and East Asia. In the NAI (NAW) weather regime, a band of dry (wet) anomalies form over midlatitude continents, while positive (negative) precipitation anomalies appear near Greenland and East Asia. In the EUI (EUW) regime, scattered dry (wet) anomalies form over northeast Pacific, and meanwhile wet (dry) anomalies appear over the Norwegian Sea and Kara-Barents Seas.

The frequency of stratospheric regimes for SSWs and SPVs is compared and the stratospheric extremes show varying preference of regimes in different stages. The regime is relatively uniform in the initial and decaying stages of SSWs, while the HW and NAW weather regimes appear the most in the onset and mature stages of SSWs. The HW regime exists the least for each period of SPVs, while the HI regime is present the most during the development and decaying periods. The other four regimes share a nearly equal chance of occurrence in the whole life cycle of SPVs.

This study has confirmed the robustness of the six stratospheric regimes identified from the observations [6] using historical simulations. However, it is still unknown to what extent the stratospheric regimes can be forecasted in operational forecast models. Precursors for the six stratospheric regimes are also still not well understood yet, left for a deep investigation in the future.

Author Contributions: Conceptualization, D.G. and Z.L.; methodology, Z.L.; software, Z.L. and Q.G.; validation, D.G. and Q.L.; formal analysis, Z.L., Q.Z. and S.Y.; investigation, Q.G.; writing—original draft preparation, Z.L.; writing—review and editing, D.G.; visualization, Q.L.; supervision, D.G.; project administration, D.G. All authors have read and agreed to the published version of the manuscript.

Funding: This work was supported jointly by grants from the National Key Research and Development Program of China (Grant No., 2022YFF0801703), the National Natural Science Foundation of China (Grant No., 42192512), and National Natural Science Foundation of China major research program (Grant No., 91837311).

Institutional Review Board Statement: Not Applicable.

Informed Consent Statement: Not Applicable.

Data Availability Statement: Not Applicable.

Acknowledgments: The authors acknowledge the ESGF (https://esgf-node.llnl.gov/projects/esgf-llnl/, accessed on 1 December 2022) for their freely providing the CMIP6 simulation. The CMIP6 data applied in our study are all public. We acknowledge the High Performance Computing Center of Nanjing University of Information Science & Technology for their support of this work.

Conflicts of Interest: The authors declare no conflict of interest.

References

1. Rao, J.; Ren, R.; Chen, H.; Yu, Y.; Zhou, Y. The stratospheric sudden warming event in February 2018 and its prediction by a climate system model. *J. Geophys. Res. Atmos.* **2018**, *123*, 13332–13345. [CrossRef]
2. Polvani, L.M.; Waugh, D.W. Upward wave activity flux as a precursor to extreme stratospheric events and subsequent anomalous surface weather regimes. *J. Clim.* **2004**, *17*, 3548–3554. [CrossRef]
3. Lu, Q.; Rao, J.; Guo, D.; Yu, M.; Yu, Y. Downward propagation of sudden stratospheric warming signals and the local environment in the Beijing-Tianjin-Hebei region: A comparative study of the 2018 and 2019 winter cases. *Atmos. Res.* **2021**, *254*, 105514. [CrossRef]
4. Scaife, A.A.; Knight, J.R.; Vallis, G.K.; Folland, C.K. A stratospheric influence on the winter NAO and North Atlantic surface climate. *Geophys. Res. Lett.* **2005**, *32*, L18715. [CrossRef]
5. Thompson, D.W.J.; Baldwin, M.P.; Solomon, S. Stratosphere-Troposphere Coupling in the Southern Hemisphere. *J. Atmos. Sci.* **2005**, *62*, 708–715. [CrossRef]
6. Liang, Z.; Rao, J.; Guo, D.; Lu, Q.; Shi, C. Northern winter stratospheric polar vortex regimes and their possible influence on the extratropical troposphere. *Clim. Dyn.* **2022**, 1–20. [CrossRef]
7. Huang, W.; Yu, Y.; Yin, Z.; Chen, H.; Gao, M. Appreciable role of stratospheric polar vortex in the abnormal diffusion of air pollutant in North China in 2015/2016 winter and implications for prediction. *Atmos. Environ.* **2021**, *259*, 118549. [CrossRef]
8. Lu, Q.; Rao, J.; Shi, C.; Guo, D.; Fu, G.; Wang, J.; Liang, Z. Possible influence of sudden stratospheric warmings on the atmospheric environment in the Beijing-Tianjin-Hebei region. *Atmos. Chem. Phys.* **2022**, *22*, 13087–13102. [CrossRef]
9. Lu, Q.; Rao, J.; Shi, C.; Guo, D.; Wang, J.; Liang, Z.; Wang, T. Observational subseasonal variability of the PM2.5 concentration in the Beijing-Tianjin-Hebei area during the January 2021 sudden stratospheric warming. *Adv. Atmos. Sci.* **2022**, *39*, 1623–1636. [CrossRef] [PubMed]
10. Manney, G.L.; Livesey, N.J.; Santee, M.L.; Froidevaux, L.; Lambert, A.; Lawrence, Z.D.; Millán, L.F.; Neu, J.L.; Read, W.G.; Schwartz, M.J.; et al. Record-Low Arctic stratospheric ozone in 2020: MLS observations of chemical processes and comparisons with previous extreme winters. *Geophys. Res. Lett.* **2020**, *47*, e2020GL089063. [CrossRef]
11. Rao, J.; Garfinkel, C.I. The strong stratospheric polar vortex in March 2020 in Sub-Seasonal to Seasonal Models: Implications for empirical prediction of the low Arctic total ozone extreme. *J. Geophys. Res. Atmos.* **2021**, *126*, e2020JD034190. [CrossRef]
12. Rao, J.; Garfinkel, C.I.; White, I.P. Predicting the downward and surface influence of the February 2018 and January 2019 sudden stratospheric warming events in Subseasonal to Seasonal (S2S) Models. *J. Geophys. Res. Atmos.* **2020**, *125*, e2019JD031919. [CrossRef] [PubMed]
13. Yu, S.; Rao, J.; Guo, D. Arctic ozone loss in early spring and its impact on the stratosphere-troposphere coupling. *Earth Planet. Phys.* **2022**, *6*, 177–190. [CrossRef]
14. Charlton, A.J.; Polvani, L.M. A new look at stratospheric sudden warmings. Part I: Climatology and modeling benchmarks. *J. Clim.* **2007**, *20*, 449–469. [CrossRef]
15. Butler, A.H.; Seidel, D.J.; Hardiman, S.C.; Butchart, N.; Birner, T.; Match, A. Defining sudden stratospheric warmings. *Bull. Am. Meteor. Soc.* **2015**, *96*, 1913–1928. [CrossRef]
16. Baldwin, M.P.; Ayarzagüena, B.; Birner, T.; Butchart, N.; Butler, A.H.; Charlton-Perez, A.J.; Domeisen, D.I.V.; Garfinkel, C.I.; Garny, H.; Gerber, E.P.; et al. Sudden stratospheric warmings. *Rev. Geophys.* **2021**, *59*, e2020RG000708. [CrossRef]
17. Baldwin, M.P.; Stephenson, D.B.; Thompson, D.W.J.; Dunkerton, T.J.; Charlton, A.J.; O'Neill, A. Stratospheric memory and skill of extended-range weather forecasts. *Science* **2003**, *301*, 636–640. [CrossRef]
18. Sigmond, M.; Scinocca, J.F.; Kharin, V.V.; Shepherd, T.G. Enhanced seasonal forecast skill following stratospheric sudden warmings. *Nat. Geosci.* **2013**, *6*, 98–102. [CrossRef]
19. Tripathi, O.P.; Baldwin, M.; Charlton-Perez, A.; Charron, M.; Cheung, J.C.H.; Eckermann, S.D.; Gerber, E.; Jackson, D.R.; Kuroda, Y.; Lang, A.; et al. Examining the predictability of the stratospheric sudden warming of January 2013 using multiple NWP systems. *Mon. Weather Rev.* **2016**, *144*, 1935–1960. [CrossRef]
20. Tripathi, O.P.; Baldwin, M.; Charlton-Perez, A.; Charron, M.; Eckermann, S.D.; Gerber, E.; Harrison, R.G.; Jackson, D.R.; Kim, B.M.; Kuroda, Y.; et al. The predictability of the extratropical stratosphere on monthly time-scales and its impact on the skill of tropospheric forecasts. *Q. J. R. Meteorol. Soc.* **2015**, *141*, 987–1003. [CrossRef]
21. Domeisen, D.I.V.; Butler, A.H.; Charlton-Perez, A.J.; Ayarzagüena, B.; Baldwin, M.P.; Dunn-Sigouin, E.; Furtado, J.C.; Garfinkel, C.I.; Hitchcock, P.; Karpechko, A.Y.; et al. The role of the stratosphere in subseasonal to seasonal prediction: 1. Predictability of the stratosphere. *J. Geophys. Res. Atmos.* **2020**, *125*, e2019JD030920. [CrossRef]
22. Domeisen, D.I.V.; Butler, A.H.; Charlton-Perez, A.J.; Ayarzagüena, B.; Baldwin, M.P.; Dunn-Sigouin, E.; Furtado, J.C.; Garfinkel, C.I.; Hitchcock, P.; Karpechko, A.Y.; et al. The role of the stratosphere in subseasonal to seasonal prediction: 2. Predictability arising from stratosphere-troposphere coupling. *J. Geophys. Res. Atmos.* **2020**, *125*, e2019JD030923. [CrossRef]
23. Scaife, A.A.; Baldwin, M.P.; Butler, A.H.; Charlton-Perez, A.J.; Domeisen, D.I.V.; Garfinkel, C.I.; Hardiman, S.C.; Haynes, P.; Karpechko, A.Y.; Lim, E.P.; et al. Long-range prediction and the stratosphere. *Atmos. Chem. Phys.* **2022**, *22*, 2601–2623. [CrossRef]
24. Kolstad, E.W.; Charlton-Perez, A.J. Observed and simulated precursors of stratospheric polar vortex anomalies in the Northern Hemisphere. *Clim. Dyn.* **2010**, *37*, 1443–1456. [CrossRef]

25. Charlton-Perez, A.J.; Ferranti, L.; Lee, R.W. The influence of the stratospheric state on North Atlantic weather regimes. *Q. J. R. Meteorol. Soc.* **2018**, *144*, 1140–1151. [CrossRef]
26. Lee, S.H.; Lawrence, Z.D.; Butler, A.H.; Karpechko, A.Y. Seasonal forecasts of the exceptional Northern Hemisphere Winter of 2020. *Geophys. Res. Lett.* **2020**, *47*, e2020GL090328. [CrossRef]
27. Lee, S.H.; Furtado, J.C.; Charlton-Perez, A.J. Wintertime North American weather regimes and the Arctic stratospheric polar vortex. *Geophys. Res. Lett.* **2019**, *46*, 14892–14900. [CrossRef]
28. Michelangeli, P.-A.; Vautard, R.; Legras, B. Weather regimes: Recurrence and quasi stationarity. *J. Atmos. Sci.* **1995**, *52*, 1237–1256. [CrossRef]
29. Grams, C.M.; Beerli, R.; Pfenninger, S.; Staffell, I.; Wernli, H. Balancing Europe's wind power output through spatial deployment informed by weather regimes. *Nat. Clim. Chang.* **2017**, *7*, 557–562. [CrossRef]
30. Ferranti, L.; Magnusson, L.; Vitart, F.; Richardson, D.S. How far in advance can we predict changes in large-scale flow leading to severe cold conditions over Europe? *Q. J. R. Meteorol. Soc.* **2018**, *144*, 1788–1802. [CrossRef]
31. Domeisen, D.I.V.; Grams, C.M.; Papritz, L. The role of North Atlantic-European weather regimes in the surface impact of sudden stratospheric warming events. *Weather Clim. Dyn.* **2020**, *1*, 373–388. [CrossRef]
32. Furtado, J.C.; Cohen, J.; Becker, E.J.; Collins, D.C. Evaluating the relationship between sudden stratospheric warmings and tropospheric weather regimes in the NMME phase-2 models. *Clim. Dyn.* **2021**, *56*, 2321–2338. [CrossRef]
33. Kretschmer, M.; Cohen, J.; Matthias, V.; Runge, J.; Coumou, D. The different stratospheric influence on cold-extremes in Eurasia and North America. *NPJ Clim. Atmos. Sci.* **2018**, *1*, 44. [CrossRef]
34. Cohen, J.; Agel, L.; Barlow, M.; Garfinkel, C.I.; White, I. Linking Arctic variability and change with extreme winter weather in the United States. *Science* **2021**, *373*, 1116–1121. [CrossRef]
35. Manzini, E.; Karpechko, A.Y.; Anstey, J.; Baldwin, M.P.; Black, R.X.; Cagnazzo, C.; Calvo, N.; Charlton-Perez, A.; Christiansen, B.; Davini, P.; et al. Northern winter climate change: Assessment of uncertainty in CMIP5 projections related to stratosphere-troposphere coupling. *J. Geophys. Res. Atmos.* **2014**, *119*, 7979–7998. [CrossRef]
36. Seviour, W.J.M.; Gray, L.J.; Mitchell, D.M. Stratospheric polar vortex splits and displacements in the high-top CMIP5 climate models. *J. Geophys. Res. Atmos.* **2016**, *121*, 1400–1413. [CrossRef]
37. Cao, C.; Chen, Y.-H.; Rao, J.; Liu, S.-M.; Li, S.-Y.; Ma, M.-H.; Wang, Y.-B. Statistical characteristics of major sudden stratospheric warming events in CESM1-WACCM: A comparison with the JRA55 and NCEP/NCAR reanalyses. *Atmosphere* **2019**, *10*, 519. [CrossRef]
38. Rao, J.; Garfinkel, C.I. CMIP5/6 models project little change in the statistical characteristics of sudden stratospheric warmings in the 21st century. *Environ. Res. Lett.* **2021**, *16*, 034024. [CrossRef]
39. Liang, Z.; Rao, J.; Guo, D.; Lu, Q. Simulation and projection of the sudden stratospheric warming events in different scenarios by CESM2-WACCM. *Clim. Dyn.* **2022**, *59*, 3741–3761. [CrossRef]
40. Liu, S.-M.; Chen, Y.-H.; Rao, J.; Cao, C.; Li, S.-Y.; Ma, M.-H.; Wang, Y.-B. Parallel comparison of major sudden stratospheric warming events in CESM1-WACCM and CESM2-WACCM. *Atmosphere* **2019**, *10*, 679. [CrossRef]
41. Gettelman, A.; Hannay, C.; Bacmeister, J.T.; Neale, R.B.; Pendergrass, A.G.; Danabasoglu, G.; Lamarque, J.-F.; Fasullo, J.T.; Bailey, D.A.; Lawrence, D.M.; et al. High climate sensitivity in the Community Earth System Model Version 2 (CESM2). *Geophys. Res. Lett.* **2019**, *46*, 8329–8337. [CrossRef]
42. Wu, Z.; Reichler, T. Variations in the frequency of stratospheric sudden warmings in CMIP5 and CMIP6 and possible causes. *J. Clim.* **2020**, *33*, 10305–10320. [CrossRef]
43. Eyring, V.; Bony, S.; Meehl, G.A.; Senior, C.A.; Stevens, B.; Stouffer, R.J.; Taylor, K.E. Overview of the Coupled Model Intercomparison Project Phase 6 (CMIP6) experimental design and organization. *Geosci. Model Dev.* **2016**, *9*, 1937–1958. [CrossRef]
44. Lu, H.; Bracegirdle, T.J.; Phillips, T.; Bushell, A.; Gray, L. Mechanisms for the Holton-Tan relationship and its decadal variation. *J. Geophys. Res. Atmos.* **2014**, *119*, 2811–2830. [CrossRef]
45. Andrews, D.G.; Holton, J.R.; Leovy, C.B. *Middle Atmosphere Dynamics*; Academic Press: San Diego, CA, USA, 1987; p. 489.
46. Rao, J.; Garfinkel, C.I.; Wu, T.; Lu, Y.; Chu, M. Mean state of the Northern Hemisphere stratospheric polar vortex in three generations of CMIP models. *J. Clim.* **2022**, *35*, 4603–4625. [CrossRef]
47. Martineau, P.; Son, S.-W. Onset of circulation anomalies during stratospheric vortex weakening events: The role of planetary-scale waves. *J. Clim.* **2015**, *28*, 7347–7370. [CrossRef]
48. Huang, J.; Tian, W.; Gray, L.J.; Zhang, J.; Li, Y.; Luo, J.; Tian, H. Preconditioning of Arctic stratospheric polar vortex shift events. *J. Clim.* **2018**, *31*, 5417–5436. [CrossRef]
49. Huang, J.; Tian, W.; Zhang, J.; Huang, Q.; Tian, H.; Luo, J. The connection between extreme stratospheric polar vortex events and tropospheric blockings. *Q. J. R. Meteorol. Soc.* **2017**, *143*, 1148–1164. [CrossRef]
50. Martineau, P.; Son, S.-W. Planetary-scale wave activity as a source of varying tropospheric response to stratospheric sudden warming events: A case study. *J. Geophys. Res. Atmos.* **2013**, *118*, 10994–11006. [CrossRef]

Disclaimer/Publisher's Note: The statements, opinions and data contained in all publications are solely those of the individual author(s) and contributor(s) and not of MDPI and/or the editor(s). MDPI and/or the editor(s) disclaim responsibility for any injury to people or property resulting from any ideas, methods, instructions or products referred to in the content.